

Na-O anticorrelation and HB

I. The Na-O anticorrelation in NGC 2808^{*,**}

E. Carretta¹, A. Bragaglia¹, R. G. Gratton², F. Leone³, A. Recio-Blanco⁴, and S. Lucatello²

¹ INAF – Osservatorio Astronomico di Bologna, via Ranzani 1, 40127 Bologna, Italy
e-mail: eugenio.carretta@oabo.inaf.it

² INAF – Osservatorio Astronomico di Padova, vicolo dell'Osservatorio 5, 35122 Padova, Italy

³ INAF – Osservatorio Astrofisico di Catania, via S. Sofia 78, 95123 Catania, Italy

⁴ Dpt. Cassiopée, UMR 6202, Observatoire de la Côte d'Azur, BP 4229, 06304 Nice Cedex 04, France

Received 18 October 2005 / Accepted 28 November 2005

ABSTRACT

We derived the atmospheric parameters and elemental abundances of Fe, O, and Na for about 120 red giant stars in the Galactic globular cluster NGC 2808. Our results are based on the analysis of medium-high resolution ($R = 22\,000\text{--}24\,000$) GIRAFFE spectra acquired with the FLAMES spectrograph at VLT-UT2 as a part of a project aimed at studying the Na-O anticorrelation as a function of physical parameters in globular clusters. We present the anticorrelation of Na and O abundances in NGC 2808 here, and discuss the distribution function of stars along this relation. Besides a bulk of O-normal stars with the typical composition of field halo stars, NGC 2808 seems to host two other groups of O-poor and super O-poor stars. In this regard, NGC 2808 is similar to M 13, the template cluster for the Na-O anticorrelation. However, in contrast to M 13, most stars in NGC 2808 are O-rich. This might be related to the horizontal branch morphologies that are very different in these two clusters. The average metallicity we found for NGC 2808 is $[\text{Fe}/\text{H}] = -1.10$ (rms = 0.065 dex, from 123 stars). We also found some evidence of a small intrinsic spread in metallicity, but more definitive conclusions are hampered by the presence of a small differential reddening.

Key words. stars: abundances – stars: atmospheres – stars: Population II – Galaxy: globular clusters: general – Galaxy: globular clusters: individual: NGC 2808

1. Introduction

This is the first paper in a series aimed at uncovering and studying the possible existence of a second generation of stars in Galactic globular clusters (GCs). The presence and the properties of these stars, probably born out of the ejecta of intermediate mass stars, can be inferred from the analysis of the Na-O anticorrelation, found and extensively studied in a number of GCs mainly by the Lick-Texas group (Kraft, Sneden and coworkers; see Gratton et al. 2004 for a recent review and a summary of abundance variations in clusters).

The Lick-Texas group found that in most of the surveyed GCs there is a star-to-star anticorrelation between the O and Na abundances. This is a sign of the (unexpected) presence of material processed through the complete CNO cycle in GC stars: at the temperature where this occurs, ^{22}Ne is transformed into ^{23}Na by proton capture (Denisenkov & Denisenkova 1989;

Langer et al. 1993). Hence, enhanced Na abundances should accompany O depletions in stars. While early interpretations called for deep mixing processes in the same stars where abundance anomalies are observed, Gratton et al. (2001) and subsequently Carretta et al. (2004b) show that the CNO cycle processed material must be due to pollution from ejecta of other (more massive) stars, since the Na-O anticorrelation is also found among unevolved stars in clusters of any metallicity (NGC 6397, NGC 6752, 47 Tuc were studied).

Favorite nucleosynthesis sites are thermally pulsating intermediate-mass asymptotic giant branch (AGB) stars undergoing hot bottom burning (Ventura et al. 2001). It is unlikely that the Na-rich, O-poor material was acquired by the stars after their formation (Cohen et al. 2002), because the accreted surface layers would be washed out by the deepening of the convective envelope during the red giant evolutionary phase. Hence, this anticorrelation most probably calls for a second generation of stars, formed within GCs from the kinematically cool ejecta of massive AGB stars (Cottrell & Da Costa 1981).

The age difference between the two populations (a few 10^8 yr) is too small to be directly detectable as different

* Based on observations collected at ESO VLT-UT2 under programme 72.D-0507.

** Complete Tables 2, 3 and 5 are only available in electronic form at <http://www.edpsciences.org>

Turn-Offs (TO's) in the color-magnitude diagrams. However, we might expect a connection between the distribution of stars along the Na-O anticorrelation and the – so far – unexplained presence of extended blue horizontal branches (BHBs) in several GCs. In fact, O-poor, Na-rich (i.e., polluted) stars should also be enriched in He (by about $\Delta Y = 0.04$: D'Antona et al. 2002). In turn, He-rich stars evolve faster on the main sequence (MS), so that polluted stars currently at the TO should be less massive (by about $0.05 M_{\odot}$) than the “normal” He-poorer stars. If these stars lost mass at the same rate as normal stars on the red giant branch (RGB), their descendants should become much hotter HB stars, maybe explaining the long blue tails observed in many GCs, e.g. in M 13 and NGC 6752, which display the most extended Na-O anticorrelations.

However, this connection still needs to be statistically proven with significative samples of stars in different clusters, in order to disentangle the possible link(s) between HB morphology (extension and mass distribution) and the other parameters (like metallicity, age, and the Na-O anticorrelation distribution function, and even the close binary fraction). A first attempt was made by Carretta et al. (2003), who used data from the FLAMES Science Verification program in order to study the Na distribution along the RGB in NGC 2808, a cluster showing a well-known bimodal HB morphology, with a clump of red HB stars and a long distribution of stars on the blue side of the RR Lyrae instability strip, down to very faint magnitudes. The FLAMES multiplex capability was used to derive Na abundances for 81 RGB stars. Unfortunately, observations of O indicators were only available for a small fraction of stars with measured Na abundances, since spectra were acquired for another purpose. While we are quite confident about the *shape* of the anticorrelation, the Na or O abundances alone would not be enough to reconstruct the *distribution function* of the anticorrelation, since Na or O saturate at the edges of the distribution. On the other hand, the *ratio* Na/O does continue to vary even at extreme values along the anticorrelation.

To study the connection between the O-Na anticorrelation and the HB morphology, an adequate sample of stars in each cluster is required: assuming a flat distribution (a very rough approximation), the probability p of covering at least a fraction x of the total range using n stars is $p = 1 - x^n$. Hence, to estimate the extent of the Na-O anticorrelation with 4% accuracy at a 95% level of confidence we need to observe ~ 80 stars in each GC. About 20 GCs with a wide distribution of HB morphologies are required to confidently conclude that a connection indeed exists. To estimate the full extent of the Na-O anticorrelation, observations of stars down to $[O/Fe] \sim -1$ dex¹ are needed: this implies high resolution and high S/N observations of RGB stars.

The capabilities of VLT+FLAMES (high multiplex gain, high resolution) allow us to gather the required number statistics, both in the number of GCs and of stars studied in each GC.

¹ We use the usual spectroscopic notation: $\log n(A)$ is the abundance (by number) of element A in the usual scale where $\log n(H) = 12$; notation $[A/H]$ is the logarithmic ratio of the abundances of elements A and H in the star, minus the same quantity in the Sun.

Table 1. Log of the observations for NGC 2808. Date is UT, and exposure times are in seconds.

Grating	Date	UT _{beginning}	exptime
HR11	2004-02-16	05:35:52.011	3000
	2004-02-16	06:26:45.660	3000
	2004-02-17	05:23:11.985	2850
	2004-02-17	06:11:42.443	2850
HR13	2004-01-12	05:36:55.750	2850
	2004-01-12	06:25:25.730	2850
	2004-01-18	05:56:41.205	3000
	2004-01-18	06:47:34.701	3000

Hence, we started the present project in order to perform a systematic analysis of a large number of stars with accurate and homogeneous Na and O abundances in about 20 GCs.

In the present paper we present the method of analysis and the results obtained for NGC 2808. An outline of the observations is given in the next section. The derivation of atmospheric parameters and the analysis are discussed in Sect. 3, whereas error estimates are given in Sect. 4. Finally, Sects. 5 and 6 are devoted to the reddening and intrinsic scatter in Fe for NGC 2808 and to the results for the Na-O anticorrelation, respectively. The summary and conclusions are presented in Sect. 7.

2. Observations

Our data were collected with the ESO high-resolution multi-fiber spectrograph FLAMES/GIRAFFE (Pasquini et al. 2002), mounted on VLT UT2. Observations were done with two GIRAFFE setups, the high-resolution gratings HR11 (centred at 5728 Å) and HR13 (centred at 6273 Å) to measure the Na doublets at 5682–5688 Å and 6154–6160 Å and the [O I] forbidden lines at 6300 and 6363 Å, respectively. Resolution is $R = 24\,200$ (for HR11) and $R = 22\,500$ (for HR13), at the centre of spectra.

We obtained 4 exposures for each grating (for both gratings, 2 exposures of 3000 s, and 2 of 2850 s); the observation log is given in Table 1. Pointings were centered at RA = 09:12:00.1, Dec = –64:51:50.7 (J2000).

Stars were selected from the photometry by Bedin et al. (2000), kindly made available by the authors and already used for a FLAMES Science Verification program (Carretta et al. 2003, 2004a). We chose stars along the RGB, from about $V = 13.9$ (1 mag below the RGB tip) down to $V = 15.5$. Targets were selected among isolated stars, i.e. all stars were chosen to be free from any companion that was closer than 2 arcsec and brighter than $V + 2$ mag, where V is the target magnitude.

We decided to target different objects with the UVES fibers, in order to observe up to 14 stars per cluster in the highest resolution mode²; hence, the GIRAFFE fiber positioning was also slightly different between the pointings used with the two gratings. As a consequence, not all the stars were observed in both gratings; on a grand total of 130 different stars observed, we

² The analysis of these higher resolution spectra will be presented elsewhere.

Table 2. List and relevant information for the target stars observed in NGC 2808. ID, B , V , and coordinates (J2000) are taken from Bedin et al. (2000); J , K are from the 2MASS catalog; radial velocities RV 's (in km s^{-1}) from both gratings are heliocentric; stars with “*” in notes have $V - K$ colours that deviate from the ones expected for RGB stars (see text). The complete table is available electronically; we show here a few lines for guidance.

Star	RA (h m s)	Dec (d p s)	V	B	J	K	$RV(\text{HR11})$	$RV(\text{HR13})$	HR	Notes
7183	9 12 2.8710	-64 49 34.069	14.854	16.168			106.58	106.55	11,13	
7315	9 11 58.581	-64 49 29.88	14.683	15.930	12.255	11.425	98.30	98.97	11,13	
7536	9 12 31.7065	-64 49 22.268	14.372	15.812	11.802	10.829		96.77	13	
7558	9 12 20.1287	-64 49 21.891	15.389	16.576	13.160	12.407	117.01	118.12	11,13	
7788	9 11 57.1979	-64 49 14.551	14.870	16.168	12.472	11.623	98.91		11	
8198	9 11 48.9714	-64 48 59.526	15.340	16.572	13.042	12.277	100.09		11	
8204	9 11 58.577	-64 48 59.27	15.119	16.397	12.793	11.879	109.67	109.95	11,13	
8603	9 12 14.0510	-64 48 42.915	14.432	15.847	11.902	10.957	109.93		11	
8679	9 11 44.5585	-64 48 39.890	14.961	16.164	12.753	12.022		43.27	13	Field

have 65 objects with spectra for both gratings, 34 with only HR11 observations and 31 with only HR13 observations. Since the Na doublet at 6154–6160 Å falls into the spectral range covered by HR13, we could measure Na abundances for all 130 target stars, whereas we could expect to measure O abundances only up to a maximum of 65+31 stars. A list of all observed targets is given in Table 2, and the colour magnitude diagram (CMD) is shown in Fig. 1.

3. Atmospheric parameters and analysis

3.1. Atmospheric parameters

Temperatures and gravities were derived as described in Carretta et al. (2003); along with the derived atmospheric parameters and iron abundances, they are shown in Table 3 (completely available only in electronic form). We used K magnitudes taken from the Point Source Catalogue of 2MASS (Cutri et al. 2003); the 2MASS photometry was transformed to the TCS photometric system, as used in Alonso et al. (1999).

We obtained T_{eff} and bolometric corrections B.C. for our stars from $V - K$ colors whenever possible. We employed the relations by Alonso et al. (1999, Eqs. (4), (7) and (17), with the erratum of 2001). For NGC 2808 we adopted a distance modulus of $(m - M)_V = 15.59$ and a reddening of $E(B - V) = 0.22$ (Harris 1996, updated at <http://physun.physics.mcmaster.ca/Globular.html>), and the relations $E(V - K) = 2.75E(B - V)$, $A_V = 3.1E(B - V)$, and $A_K = 0.353E(B - V)$ (Cardelli et al. 1989). An input metallicity of $[\text{Fe}/\text{H}] = -1.14$ was adopted from Carretta et al. (2004a), based on the analysis of UVES Red Arm spectra³.

There are a few target stars with no K magnitude from 2MASS and a few others appearing as outliers in the V , $V - K$ diagram, but not in the V , $B - V$ diagram: this is probably due to the worse spatial resolution of 2MASS, an important factor in a dense GC field. Temperatures for these stars were derived from a mean relation $T_{\text{eff}}(V - K)$ as a function of $T_{\text{eff}}(B - V)$.

Surface gravities $\log g$'s were obtained from effective temperatures and bolometric corrections, assuming that the stars

³ This value is slightly different from what we derive in the present study; however, the dependence of $(V - K)$ on $[\text{Fe}/\text{H}]$ is so weak that temperatures are almost unaffected by this difference.

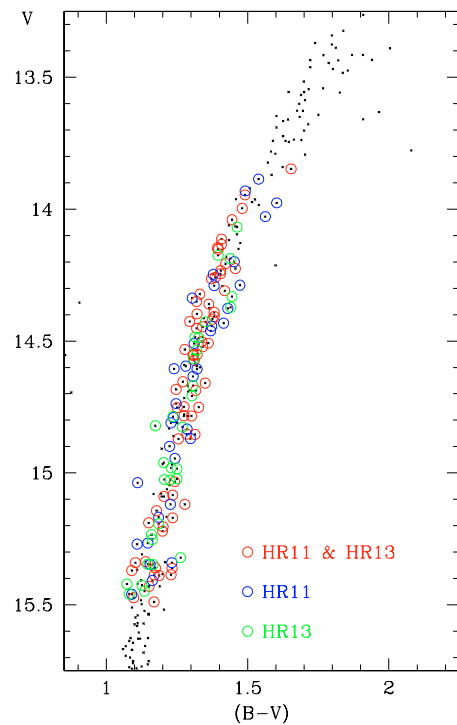


Fig. 1. The CMD of NGC 2808 (taken from Bedin et al. 2000); the targets observed with the GIRAFFE/MEDUSA gratings are indicated by open circles. The colour coding indicates the setups used in the observations (red for both HR11 and HR13, blue for HR11 only, green for HR13 only).

have masses of $0.85 M_{\odot}$. The adopted bolometric magnitude of the Sun is $M_{\text{Bol},\odot} = 4.75$.

We did not take the existence of differential reddening (Walker 1999; Bedin et al. 2000) into account, since no individual correction for each star is available in the literature. The differential reddening is, however, small: peak-to-peak differences amount to ~ 0.08 mag ($\sigma \approx 0.020$ – 0.028 ; Walker 1999; Bedin et al. 2000). The effect of this will be taken into account as an additional error source in the abundance derivation (see Sect. 4).

Table 3. Adopted atmospheric parameters and derived iron abundances of RGB stars in NGC 2808; nr indicates the number of lines used in the analysis. The complete table is available in electronic form.

Star	T_{eff} (K)	$\log g$ (dex)	[A/H] (dex)	v_t (km s ⁻¹)	nr	[Fe/H]I (dex)	rms	nr	[Fe/H]II (dex)	rms
07183	4423	1.51	-1.08	1.66	41	-1.08	0.13	3	-1.06	0.17
07315	4452	1.45	-1.24	1.54	33	-1.24	0.10	3	-1.16	0.17
07536	4247	1.18	-1.09	1.45	23	-1.08	0.13	3	-1.01	0.11
07558	4692	1.87	-1.22	1.30	33	-1.21	0.12	3	-1.17	0.18
07788	4461	1.53	-1.17	1.40	18	-1.17	0.14			
08198	4617	1.81	-1.21	1.21	13	-1.21	0.14			
08204	4467	1.63	-1.05	1.35	38	-1.05	0.15	3	-1.14	0.14
08603	4292	1.24	-1.05	1.65	19	-1.05	0.12			
08679	4734	1.72	-0.25	1.38	21		0.20	3	-0.79	0.07
08739	4213	1.13	-1.07	1.82	19	-1.07	0.12			
08826	4565	1.66	-0.99	1.22	39	-0.98	0.15	3	-0.97	0.08

3.2. Equivalent widths

Data reduction was done using standard IRAF⁴ packages for bias subtraction, flat-fielding correction, correction for scattered light, spectra extraction, and wavelength calibration. We measured radial velocities (RVs) for each spectrum (using RVIDLINES on about 25 to 40 lines for HR11 and HR13, respectively); the error is less than 0.5 km s⁻¹ on each measure, and we put in Table 2 the average for the 4 pointings in each grating, after correction for heliocentric motion. The average heliocentric velocity is $RV = 102.4 \text{ km s}^{-1}$ ($\sigma = 9.8$ from 124 stars, after eliminating the non-members on the basis of their very discrepant RVs (more than 6σ from the average)). All spectra were shifted to zero radial velocities, then combined star by star; this enhanced S/N and eliminated cosmic rays hits from the coadded spectra.

In the case of HR13, before coadding, each individual spectrum was corrected for blending with telluric lines due in particular to H₂O and O₂ near the [O I] line at 6300 Å; we checked that no correction was necessary for the [O I] line at 6363 Å, or the Na lines in HR11. We generated a synthetic spectrum covering the interval 6280 to 6325 Å, taking line positions and equivalent widths for atmospheric lines in the Sun from the tables by Moore et al. (1966). We then adjusted the spectral resolution and line strengths until they matched the resolution of GIRAFFE spectra and the intensity of telluric features at the moment of observations.

Our stellar spectra were then divided by the adjusted synthetic spectrum of the telluric lines, cleaning the [O I] line fairly well from telluric contaminations. Finally, a coadded spectrum was obtained from these cleaned spectra; the final S/N ratio is always high ($S/N > 100$, and up to 300, depending on the stellar magnitude and centering of the star on the fibre), as estimated from the averages computed in several small intervals that are free of lines along the spectra.

The blaze function was removed with standard IRAF tasks. After this, a refined continuum tracement was derived as follows. First, we summed (for each grating) the spectra of all

cluster stars; then we selected a fair number of fiducial regions of continuum in the resulting master spectrum (of very high S/N ratio). By using a specialized set of commands in the ROSA spectrum analysis package (Gratton 1988), the final continuum placement was done using these fiducial points.

Equivalent widths⁵ (EW) were measured as described in detail in Bragaglia et al. (2001); in particular, in the iterative clipping to derive a local continuum around each line, we decided after several checks that a clipping factor of 2 for stars cooler than 4600 K and a factor 1 for warmer stars was the optimal choice for NGC 2808.

3.3. Iron abundances

We started from the line list described in Gratton et al. (2003) and extensively used in the analysis of high resolution spectra of GC stars (see Carretta et al. 2004a,b; Gratton et al. 2001). Atomic parameters for the subset of lines falling in the spectral range covered by gratings HR11 and HR13 are those given in that paper, as well as the reference solar abundance that are used (computed using the Kurucz 1995 model atmospheres grid, see below).

However, the original line list was optimized for a higher resolution than the present one, so we had to cull out a few Fe I lines whose abundances were systematically discrepant, most likely because of blends. We ended up with typically 15 to 18 Fe I lines safely measurable in stars with only HR11 observations, 18 to 22 lines with only HR13 spectra, and up to 30 or 40 lines for stars observed with both gratings. The number of measured Fe II lines ranges from zero to a maximum of 4.

Values of the microturbulence velocity v_t were obtained by eliminating trends of the abundances from Fe I lines with *expected* line strength (see Magain 1984). We checked that the optimization for individual stars resulted in a much smaller scatter in the derived abundances than using a mean value of v_t as a function of T_{eff} or $\log g$. For stars with observations only in HR11, the uncertainty attached to v_t is obviously larger, since only a few lines could be used.

⁴ IRAF is distributed by the National Optical Astronomical Observatory, operated by the Association of Universities for Research in Astronomy, under contract with the National Science Foundation.

⁵ EW s are available upon request from the first author.

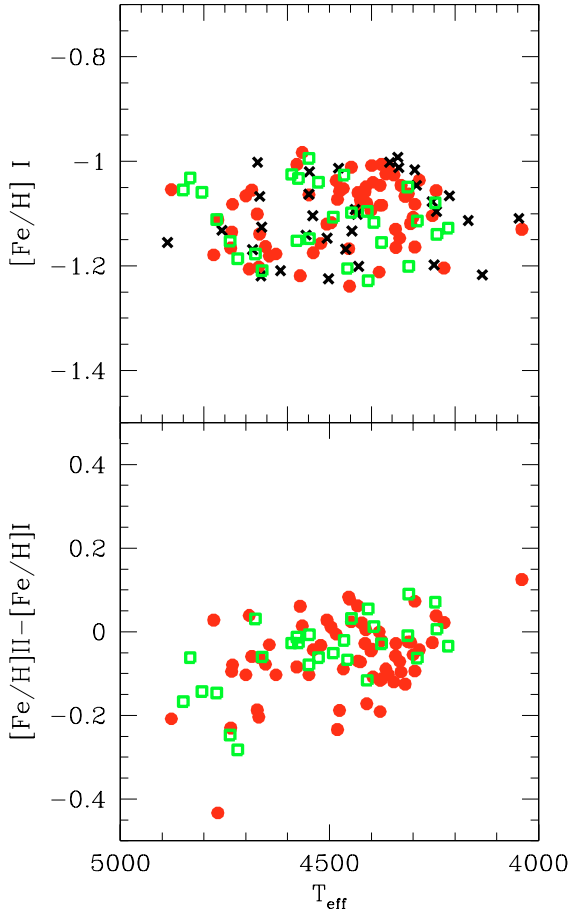


Fig. 2. Run of $[\text{Fe}/\text{H}]$ ratio and of the Iron ionization equilibrium as a function of temperatures for program stars in NGC 2808. Symbols and colour-coding refer to the setup used: (red) filled circles indicate stars with both HR11 and HR13 observations, (black) crosses for HR11 only, and (green) empty squares for HR13 only.

Final metallicities are obtained by choosing the model in the Kurucz (1995) grid of model atmospheres (with the option for overshooting on) with the proper atmospheric parameters whose abundance matches the one derived from Fe I lines. Average abundances of iron for NGC 2808 are $[\text{Fe}/\text{H}]_{\text{I}} = -1.10$ (rms = 0.065) dex, from 123 stars and $[\text{Fe}/\text{H}]_{\text{II}} = -1.16$ (rms = 0.093) dex, from 90 objects. We do not think this difference is really relevant, since abundances for Fe II rely on only two lines on average.

Our metallicity, based on the analysis of medium resolution GIRAFFE spectra for a large sample of RGB stars in NGC 2808, is in very good agreement with previous results by Carretta et al. (2004a), who derived $[\text{Fe}/\text{H}]_{\text{I}} = -1.14$ (rms = 0.06) dex and $[\text{Fe}/\text{H}]_{\text{II}} = -1.14$ (rms = 0.13) dex from a sample of 20 red giants with UVES Red Arm spectra, covering a much wider spectral range.

The distribution of resulting $[\text{Fe}/\text{H}]$ values as a function of the temperatures is shown in Fig. 2, with stars coded according to the grating they were observed with. The scatter of the metallicity distribution is discussed in Sect. 5.

3.4. Sodium and oxygen abundances

Abundances of O and Na rest on measured EWs. For Na, one or both the doublets at 5672–88 Å and at 6154–60 Å (depending on the setup observed) are always available. Derived average Na abundances were corrected for effects of departures from the LTE assumption using the prescriptions by Gratton et al. (1999).

Oxygen abundances are obtained from the forbidden [O I] lines at 6300 and 6363 Å. The O lines were carefully inspected by eye; in some cases they were measured interactively if the automatic measurement failed (e.g., because of some residual asymmetries due to imperfect removal of telluric lines). In this check we were also able to derive fairly reasonable upper limits to the EWs in a few stars.

The contribution to the forbidden [O I] line from the Ni blend at 6300.34 Å is not a source of concern: Carretta et al. (2004a) estimate that the EWs of the [O I] 6300.31 Å line in RGB stars are hardly affected by more than ~ 0.5 mÅ in NGC 2808. Also, CO formation is not expected to lead to significant corrections to the O abundances, given the rather high temperatures of the stars and the low expected C abundances.

4. Errors in the atmospheric parameters

Errors in the derived abundances are affected by three main contributions (errors in temperatures, in microturbulence velocities, and in the measurements of EWs), and by two less severe error sources: errors in surface gravities and in the adopted model metallicity. In the following, we concentrate on the major error sources.

Errors in temperatures. Bedin et al. (2000) estimate 0.02 mag (one σ) for the effect of differential reddening across the cluster area where our targets were selected. Using the calibrating relations by Alonso et al. (1999), the effect of an error of 0.02 mag in $E(B - V)$ translates into an error of 41 K in T_{eff} . On the other hand, the photometric error in the adopted $V - K$ colors is given by the quadratic sum of errors in V (estimated in a few thousandths of mag by Bedin et al.) and in K (~ 0.02 mag, from 2MASS). Since the two photometries (optical and IR) are independent, there is no color term and we adopt a photometric error of 0.02 mag in $V - K$. When summed in quadrature with the error due to the differential reddening (~ 0.05 mag in $E(V - K)$), we obtain 0.054 mag. The adopted internal error in T_{eff} is thus 44 K.

Errors in microturbulence velocities. We computed the quadratic mean of the 1σ errors in the slope of the abundance-expected line strength relation from all stars. Afterward, we used star 7183 and repeated the analysis changing v_t until the 1σ value from the original slope of the relation between line strengths and abundances was reached. A simple comparison allows us to give an estimate of 1σ error associated to v_t , which is 0.09 km s^{-1} . This error is mainly random; systematics due to blending and to the continuum tracement are negligible, and a

Table 4. Sensitivities of abundance ratios to variations in the atmospheric parameters and to errors in the equivalent widths, as computed for a typical program star with $T_{\text{eff}} = 4500$ K. The total error is computed as the quadratic sum of the three dominant sources of error, T_{eff} , v_t , and errors in the EW s (Col. 8: tot.1) or as the sum of all contributions (Col. 9: tot.2).

Ratio	ΔT_{eff} (+50 K)	$\Delta \log g$ (+0.2 dex)	$\Delta [A/H]$ (+0.10 dex)	Δv_t (+0.20 km s ⁻¹)	$\langle N_{\text{lines}} \rangle$	ΔEW	tot.1 (dex)	tot.2 (dex)
(1)	(2)	(3)	(4)	(5)	(6)	(7)	(8)	(9)
[Fe/H]I	+0.047	+0.001	-0.001	-0.029	38	+0.021	0.059	0.059
[Fe/H]II	-0.040	+0.010	+0.017	-0.011	3	+0.076	0.087	0.089
[O/Fe]I	+0.046	-0.001	+0.004	+0.009	2	+0.093	0.104	0.104
[Na/Fe]II	-0.006	-0.006	-0.020	+0.005	4	+0.066	0.066	0.070

systematic contribution from errors in the gfs is not likely, at least for iron lines.

Errors in the measurement of equivalent widths. In order to estimate this contribution, we selected a subset of 63 stars with more than 25 measured Fe lines. The average rms scatter (0.131 dex) in Fe abundance for these stars, divided by the square root of the typical average number of measured line (38), provides a typical internal error of 0.022 dex.

Table 4 shows the sensitivity of the derived abundances to variations in the adopted atmospheric parameters for Fe, Na, and O; this is obtained by re-iterating the analysis while each time varying only one of the parameters of the amount shown in the table. This exercise was done for all stars in the sample, and the average value of the slope corresponding to the average temperature (~ 4500 K) in the sample was used to estimate the internal errors in abundances. For iron, these amount to ~ 0.05 dex and 0.027 dex, due to the quoted uncertainties in T_{eff} and v_t .

The impact of errors in EW s is evaluated in Col. 7, where the average error from a single line is weighted by the square root of the mean number of lines, given in Col. 6. This is done for iron and for the other elements measured in this paper.

Total errors, computed using only the dominant terms and including all the contributions, are reported in Table 4, in Cols. 8 and 9, respectively.

5. Cosmic scatter and reddening in NGC 2808

We can now evaluate the expected scatter in [Fe/H] due to the uncertainties in T_{eff} , v_t , and errors in EW s, and we derive $\sigma_{\text{FeI}}(\text{exp.}) = 0.059 \pm 0.008$ dex (statistical error) from Table 4. The inclusion of contributions due to uncertainties in surface gravity or model metallicity does not alter our conclusions. This result can be compared to the bona fide observed scatter $\sigma_{\text{FeI}}(\text{obs.}) = 0.063 \pm 0.008$ dex (statistical error) estimated as the average rms scatter that we obtain using the 63 stars in our sample with at least 25 measured iron lines.

From the quadratic difference between observed and expected scatter, we can derive a formal value of 0.022 dex for the intrinsic spread in metallicity in NGC 2808. Taking the attached statistical errors into account, we could set a limit of $\lesssim 0.05$ dex as the maximum spread in iron abundance allowed in this cluster. Note that a $\sim 2\sigma$ evidence of a spread of ~ 0.02 dex

Table 5. Abundances of O and Na in NGC 2808. The [Na/Fe] values are corrected for departures from LTE, and HR is a flag for the grating used (1 = HR11 only, 2 = HR11 and HR13, 3 = HR13 only). Lim is a flag discriminating between real detections and upper limits in the O measurements (0 = upper limit, 1 = detection). The complete table is available electronically.

Star	nr	[O/Fe]	rms	nr	[Na/Fe]	rms	HR	lim
07183	2	+0.109	0.285	4	+0.217	0.093	2	1
07315	2	+0.384	0.041	4	-0.132	0.069	2	1
07536	2	+0.386	0.049	2	+0.004	0.067	1	1
07558	2	+0.428	0.205	2	+0.041	0.063	2	1
07788				2	+0.503	0.102	3	1
08198				2	+0.126	0.029	3	1
08204	2	+0.324	0.004	4	-0.010	0.162	2	1
08603				2	+0.052	0.143	3	1
08679	2	-0.136	0.028	2	+0.303	0.036	1	1
08739				2	+0.101	0.053	3	1
08826	1	-0.605		3	+0.470	0.167	2	1
09230				2	+0.659	0.081	3	1
09724	2	-0.171	0.091	4	+0.426	0.181	2	1
09785				2	+0.471	0.027	1	1
10012	2	-0.235	0.164	4	+0.369	0.151	2	1

seems to be present between the average abundances of Na-poor and Na-rich stars, in NGC 2808 (see below).

In summary, we believe that the dominant contribution to the spread comes from differential reddening: we are confident that the intrinsic spread is small, though perhaps not negligible. The stellar population in NGC 2808 can be considered reasonably homogeneous in Fe content, within a few hundredths of dex.

6. Results and discussion: the Na-O anticorrelation

Abundances of O and Na are listed in Table 5 (only available in electronic form) together with the number of measured lines and the rms value obtained for each species. The [Na/Fe] ratio as a function of [O/Fe] ratio is displayed in Fig. 3 for each of the red giant stars with both O and Na detections in NGC 2808, and for a few stars in which only upper limits in the EW s of the [O I] 6300 Å line were measured. The high resolution and high S/N ratio of our spectra allow us to confidently reach stars down to [O/Fe] ~ -1 .

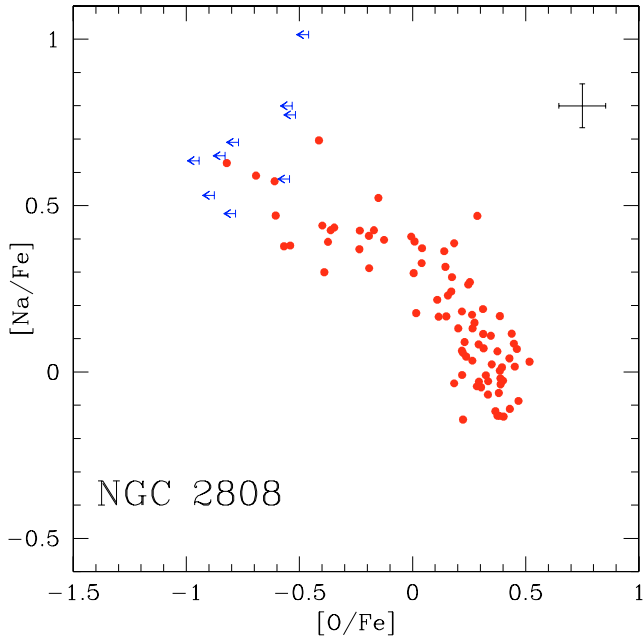


Fig. 3. The $[\text{Na}/\text{Fe}]$ ratio as a function of $[\text{O}/\text{Fe}]$ for red giant stars in NGC 2808. Na abundances do include the corrections for departures from LTE following Gratton et al. (1999). Upper limits in $[\text{O}/\text{Fe}]$ for a few stars are indicated as blue arrows. The error bars take the uncertainties in atmospheric parameters and EW s into account.

The classical Na-O anticorrelation is clearly present also in this cluster, as already shown by Carretta et al. (2004a): stars sharing the same position along the giant branch show very different O and Na content.

There is scarce – if at all – evidence of an internal origin in the very same stars that we presently observe for this phenomenon. There is no evidence that O-poor, Na-rich stars are segregated in particular regions of the sampled RGB (upper and middle panels in Fig. 4). This is at odds with expectations if evolutionary processes, due to some extra-mixing, are at work as the stars climb along the RGB, bringing to the surface more and more material processed by nuclear proton-capture reactions. The theoretical scenario would imply a bunch of heavily altered Na-rich, O-depleted stars at the bright (cool) end of the RGB. This is not seen, thus confirming early results by Carretta et al. (2003) in this cluster: the spread in abundances seen at every luminosity along the RGB tells us that, whatever the mechanism producing the alterations is, these anomalies are likely to be established well before the stars begin to move towards more advanced evolutionary phases (see also Gratton et al. 2001 and Carretta et al. 2004b for studies in scarcely evolved cluster stars).

Since Na or O saturates at the edges of the distribution function (the $[\text{O}/\text{Fe}]$ ratio, for instance, levels off to the average value typical of halo field stars, whereas $[\text{Na}/\text{Fe}]$ still varies), the ratio O/Na appears the best indicator to trace the stars’ distribution along the Na-O anticorrelation because this ratio does continue to vary even at extreme values. Excluding the non-members, we have 82 stars where O is detected and 9 others with a robust upper limit. However, we have Na abundances available for all the 123 member stars examined, thus

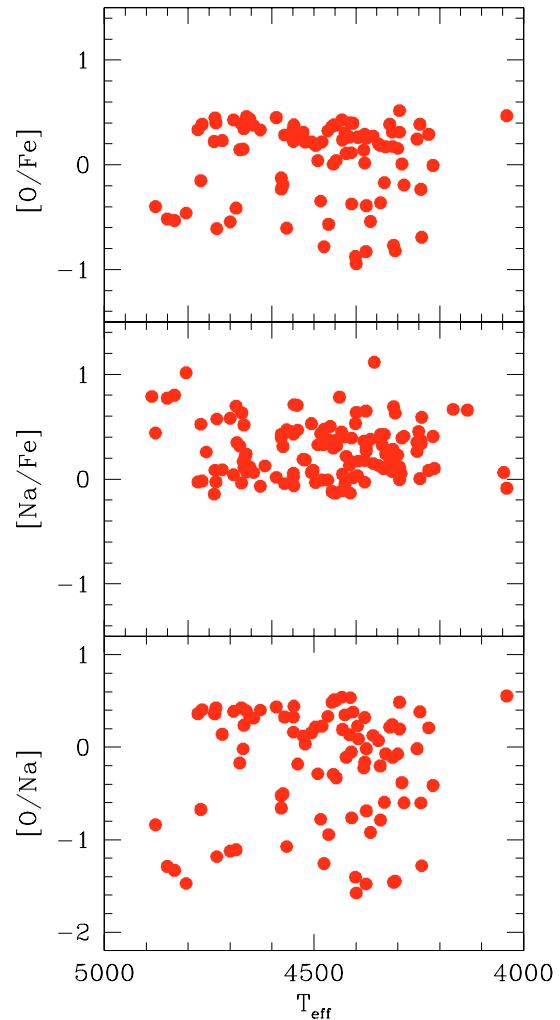


Fig. 4. Run of $[\text{O}/\text{Fe}]$ (upper panel), $[\text{Na}/\text{Fe}]$ (middle panel), and $[\text{O}/\text{Na}]$ ratios (lower panel) as a function of the evolutionary status (as represented by the effective temperature) for stars in our sample in NGC 2808.

we are able to “project” every star with no direct O determination along the locus defined by the global Na-O anticorrelation, whose shape is established very well.

This correlation is shown in Fig. 5 where the general shape of the Na-O anticorrelation is drawn using a collection of literature data for almost 400 stars in about 20 globular clusters (47 Tuc, NGC 6752, NGC 6397, M 13, M 3, M 5, NGC 3201, Ter 7, Pal 5, M 4, NGC 288, NGC 362, NGC 7006, M 15, M 10, Pal 12, M 71, NGC 6528, M 54; references and evolutionary status of the observed stars are listed in Table 6). We took, whenever stated in the original papers, the different adopted solar abundances into account, bringing them to our reference scale (Gratton et al. 2003). In this figure most of the stars (blue points) are evolved red giants, but the anticorrelation is well followed even by scarcely evolved cluster stars (about 40 turnoff and subgiant stars, red points) as well as by the RGB stars of the present study (green points).

Table 6. References for the [O/Fe] and [Na/Fe] ratios from high resolution analyses in globular clusters used to derive the overall Na-O anticorrelation shape.

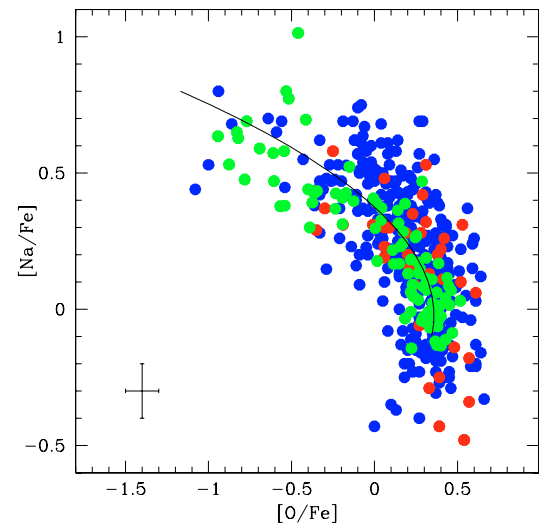
Cluster	stars	Reference
NGC 104 (47 Tuc)	SGB+TO	Carretta et al. (2004b)
	RGB	Norris & Da Costa (1995)
	RGB	Carretta (1994)
NGC 288	RGB	Shetrone & Keane (2000)
NGC 362	RGB	Shetrone & Keane (2000)
NGC 2808	RGB	Carretta et al. (2004a)
	RGB	present study
NGC 3201	RGB	Gonzalez & Wallerstein (1998)
NGC 5272 (M 3)	RGB	Cohen & Melendez (2005)
	RGB	Snedden et al. (2004)
NGC 5904 (M 5)	RGB	Ivans et al. (2001)
NGC 6121 (M 4)	RGB	Ivans et al. (1999)
NGC 6205 (M 13)	RGB+SGB+TO	Cohen & Melendez (2005)
	RGB	Snedden et al. (2004)
NGC 6254 (M 10)	RGB	Kraft et al. (1995)
NGC 6397	SGB+TO	Carretta et al. (2005) + Gratton et al. (2001)
	RGB	Norris & Da Costa (1995)
	RGB	Carretta (1994)
NGC 6528	RHB	Carretta et al. (2001)
NGC 6715 (M 54)	RGB	Brown et al. (1999)
NGC 6752	SGB+TO	Carretta et al. (2005) + Gratton et al. (2001)
	RGB	Yong et al. (2003)
	RGB	Norris & Da Costa (1995)
	RGB	Carretta (1994)
NGC 6838	RGB+SGB+TO	Ramirez & Cohen (2002)
NGC 7006	RGB	Kraft et al. (1998)
NGC 7078 (M 15)	RGB	Snedden et al. (1997)
Pal 5	RGB	Smith et al. (2002)
Pal 12	RGB	Cohen (2004)
Ter 7	RGB	Tautvaisiene et al. (2004)

Apart from providing us with an useful tool also for exploiting stars having no direct O observations, this plot suggests some interesting points:

- (i) clusters of any metallicity in the typical range of these systems are represented in this plot from M 92 ([Fe/H] = -2.16 dex, Carretta & Gratton 1997) to NGC 6528 ([Fe/H] = $+0.07$ dex, Carretta et al. 2001);
- (ii) a large range of physical properties (total mass, concentration, density) is sampled by these clusters;
- (iii) all kinds of HB morphologies (from red clump only to very extended blue HBs) are present among the clusters used to produce this plot;
- (iv) all cluster stars, irrespective of their evolutionary status (from scarcely evolved stars near the cluster turn-off to bright giants near the RGB tip), seem to follow the same locus in this plane.

Moreover, some of the studied clusters (e.g. Pal 12, M 54, Ter 7) have very likely originated in extragalactic objects, later accreted by our Galaxy.

From this evidence we can conclude safely enough that whatever the mechanism responsible, the anticorrelation must be an *intrinsic* property of a globular cluster, a universal feature of these objects. Moreover, point (iv) supports the idea that it is likely to be related to the cluster formation process itself, since it is already in place among unevolved stars formed in the first

**Fig. 5.** Global Na-O anticorrelation (solid black line) superimposed on a collection of stars in about 20 globular clusters. Blue points are RGB stars from literature studies; red points are scarcely evolved stars (turnoff or subgiant stars) from Gratton et al. (2001) and Carretta et al. (2004); green points are RGB stars in NGC 2808 from the present study.

few 10^7 – 10^8 years from the beginning of the star formation in each cluster.

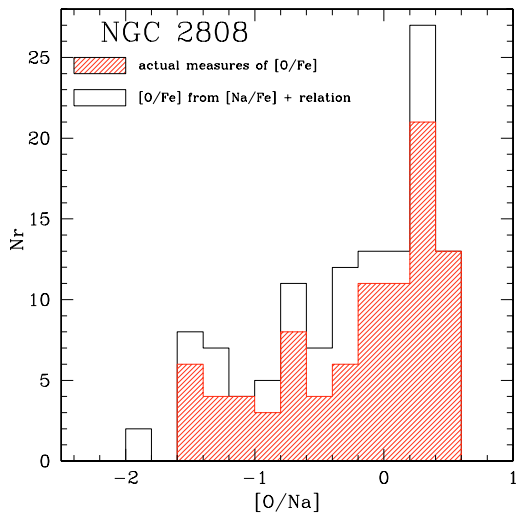


Fig. 6. Distribution function of the $[O/Na]$ ratios along the Na-O anticorrelation in NGC 2808. The dashed area is the frequency histogram referred to actual detection of O in stars, whereas the empty histogram is obtained by using the global anticorrelation relationship to obtain abundances of O also for stars with no observation with HR13 and/or only upper limit in O abundance.

In fact, unevolved low mass stars do not reach the high temperatures required for activating proton capture chains such as the NeNa and MgAl; moreover they do not possess efficient convective envelopes. It follows that any variations in the abundances of p -capture elements (O, Na, Mg, Al) must very likely be already imprinted in the gas out of which these stars formed. The typical times for the release of ejecta enriched in these elements (such as those from the most favorite candidate polluters – intermediate-mass AGB stars – see Gratton et al. 2004 and Carretta et al. 2005 for a detailed discussion) are just a few 10^7 – 10^8 years, since these are among the first objects to evolve and die in a globular clusters (see also D’Antona et al. 2005).

The distribution function of stars along the Na-O anticorrelation in NGC 2808 is shown in Fig. 6, where the ratio $[O/Na]$ from our data is used. The dashed area shows the distribution obtained by using only actual detections or carefully checked upper limits. The empty histogram is derived by following the overall Na-O anticorrelation, in order to get $[O/Fe]$ values even for stars with no observations in HR13.

The bulk of stars along the RGB in NGC 2808 is peaked at $[O/Fe] \sim 0.28$ (and $[O/Na] \sim 0.17$ dex) with a scatter of 0.12 dex around this value; this should represent the “normal” O content of the ejecta by massive, type II supernovae (SNe), typical of halo objects. We can identify this group of stars as the counterpart of the general halo field objects.

However, the distribution of stars continues down to very low $[O/Na]$ values in NGC 2808. A clearcut division into well-defined groups is rather hard to apply, since the appearance of the distribution is more like an extended tail, starting from normal-halo O values. However, if we take as a working hypothesis $[O/Na] = -0.3$ and -1.0 as boundaries, we can tentatively identify two other groups of O-poor and super O-poor stars, peaking at $[O/Fe]$, $[O/Na] = -0.21, -0.62$ and $-0.73, -1.40$ dex, respectively.

Although the statistical significance is admittedly not very high (the rms scatter in each group is about 0.2 dex), the average Fe abundance is increasing, going from $[Fe/H] = -1.113 \pm 0.008$ ($\sigma = 0.067$ dex, 74 stars) in the group of O-normal stars, to $[Fe/H] = -1.104 \pm 0.011$ ($\sigma = 0.052$ dex, 27 stars) and $[Fe/H] = -1.079 \pm 0.014$ ($\sigma = 0.064$ dex, 21 stars) for the O-poor and super O-poor groups. This is very interesting, since it is in qualitative agreement with what we expect if O-depleted stars are also enriched in He probably from the same polluting source (intermediate-mass AGB stars?). In fact, in stars with the same original metal abundance, an increase in He abundance would be seen as an increased strength of metallic lines (Böhm-Vitense 1979).

This is exactly the trend that we observe in NGC 2808, even if more significative conclusions on the intrinsic Fe spread are hampered by the presence of a small differential reddening in this cluster. However, this effect of decreasing Fe cannot be explained by it, which would instead produce fluctuations around a mean value.

Vice versa, we can reverse this line of thought and ask what mass fraction Y of He may be associated to these three groups, simply starting from the definition of the logarithmic ratio $[Fe/H]$, assuming the number of H atoms proportional to the mass fraction X and neglecting the contribution of heavy species Z . We found that in order to reproduce the different $[Fe/H]$ between the O-normal group (probably with a primordial $Y = 0.24$) and the super O-poor group, we need to consider a value $Y = 0.30$ for the latter. The intermediate group should have a mass fraction Y of about 0.26.

Interestingly, we do not find any evidence of a group having a large He enrichment, about $Y = 0.40$: this would correspond to a mean value of $[Fe/H] \sim -1.010$ dex, 0.1 dex more metal-rich than the dominant population. This would exceed the intrinsic scatter carefully evaluated in Sect. 5. If confirmed, this would put strong constraints on every model concerning star formation, in one or multiple generations in a globular cluster. In particular, the model proposed very recently by D’Antona et al. (2005) predicts that about 20% of stars are generated in a stage of star formation from ejecta of massive AGB stars with $Y = 0.40$. We would expect to also reveal such stars along the RGB. However, very He-enriched stars would have a turnoff mass that is lower than about $0.65 M_{\odot}$ (D’Antona et al. 2005), and if the mass loss rate does not depend strongly on Y , these stars could have left the RGB before reaching the He-flash point. In this case, these objects could not be really represented in our observed sample.

Notice also that the fractions we found for the different groups on the RGB support this view. From the numbers of stars in the RHB and BHB of NGC 2808, as reported in D’Antona & Caloi (2004) and from the histogram in their Fig. 1, we derived a ratio 1:0.65:0.38 for the RHB clump, the so-called EBT1 (the bulk of stars at brighter magnitudes in the BHB) and the sum of stars in the EBT2+EBT3 groups (the faint part of the BHB, see Bedin et al. 2000). As explained in the modeling by D’Antona et al. (2005), these are the likely outcome of stars starting their life with a He mass fraction $Y = 0.24, \sim 0.27$ and 0.40 , respectively.

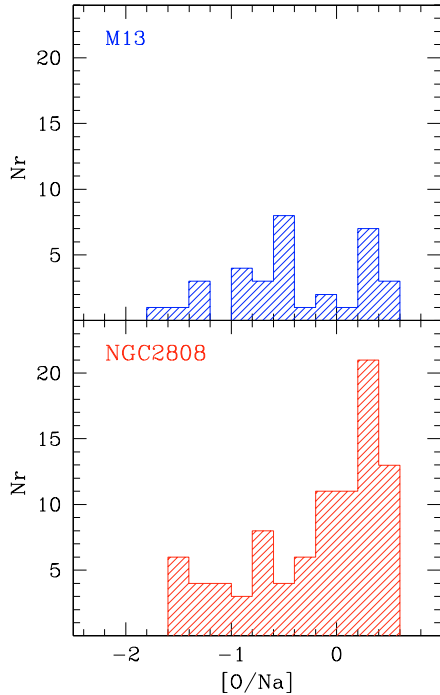


Fig. 7. Distribution function of the measured $[O/Na]$ ratios along the Na-O anticorrelation in M 13 (Sneden et al. 2004) and NGC 2808. The O and Na abundances in M 13 are shifted to our scale by correcting for different adopted solar abundances; for M 13 we used the Na abundances corrected for departures from LTE.

On the other hand, following the above discussion, we can infer that in our sample along the RGB in NGC 2808 we found 74 O-normal stars, probably with a (“cosmological”) He content $Y = 0.24$ and 27+21 stars in the O-poor and super O-poor subgroups, respectively, with Y increasing up to $Y = 0.30$. In these cases the ratio is again 1:0.65 for the O-normal:(O-poor+super O-poor) populations, supporting the view that we are sampling the progenitors of RHB stars and of the bulk of brighter BHB stars. The super He-rich progenitors of the extreme BHB stars could simply be missing in our sample if they never completed their RGB evolution.

In Fig. 7 we compare the observed distributions of RGB stars along the global Na-O anticorrelation in NGC 2808 (present study) and M 13 (Sneden et al. 2004), the template cluster as far as the Na-O anticorrelation is concerned. Abundances for Na and O in M 13 are corrected for the adoption of different solar abundances from ours; for Na we used the values corrected for effects of departures from LTE using the same prescriptions by Gratton et al. (1999), as we did for NGC 2808. This (homogeneous) comparison shows that:

- in both clusters three groups of stars (O-normal, O-poor and super O-poor) can be seen distributed along the global Na-O anticorrelation. In particular, we note that M 13 is no longer the only cluster in which stars with very low O abundances can be observed. Although Sneden et al. (2004) do not distinguish between limits and actual detections, stars with $[O/Fe]$ ratios as low as ~ -1 (within the uncertainties related to the analysis) are found in both clusters;

- whatever the mechanism responsible for the anticorrelation, it produced the same range in $[O/Na]$ ratios;
- the relative weights in the distribution functions along the Na-O relation are different in the two clusters: a Kolmogorov-Smirnov test shows only a $\sim 3\%$ probability that both samples in Fig. 7 are extracted from the same parent distribution;
- at variance with M 13, most stars in NGC 2808 are O-normal. This might be related to the HB morphologies, which are very different in the two clusters: NGC 2808 has a bimodal HB (HB parameter $(B - R)/(B + V + R) = -0.49$ from the on line catalog by Harris 1996), while the HB of M 13 (HB parameter = 0.97 from the same source) is only populated to the blue of the RR Lyrae instability strip.

In NGC 2808 there seems to be a rather straightforward correspondence between the stars along the RGB and their progeny on the HB. Following the previous discussion, it seems possible to identify RHB stars as those having O-rich/Na-poor/He-poor composition when formed. The two other groups could originate the BHB, for instance, as in the scenario devised by D’Antona and coworkers.

However, the case of M 13 seems to show that more modeling is required, since a relevant group of O-normal stars is present on the RGB, yet no RHB stars are found in this cluster. Where have all the O-normal stars gone, after the He-flash, in M 13? We have to postpone a more thorough discussion to until completion of the analysis of our whole sample of clusters with different HB morphologies.

7. Summary and conclusions

In this paper we have derived atmospheric parameters and elemental abundances for about 120 red giant stars in the globular cluster NGC 2808, as follows.

- From the analysis of GIRAFFE spectra sampling the forbidden $[O\ I]$ lines and the Na doublets at 5682–88 and 6154–60 Å, we measured Na and O abundances for a large sample of stars. We also derived the distribution function of stars in $[O/Na]$, i.e. along the Na-O anticorrelation, the well-known signature of proton-capture reactions at high temperature.
- We found that the bulk of stars along the RGB in NGC 2808 has the normal O (and Na) content typical of field halo stars, where we are predominantly seeing the contributions of yields from massive type II supernovae. However, we also tentatively identified two other groups of stars whose O content is depleted or even strongly depleted.
- Evidence of accompanying He-enrichment comes from the average Fe abundances in these two groups, although the statistical significance is not very high. However, the qualitative agreement between the observations and the theoretical prediction for pollution by He-rich and O-depleted matter provided by a previous generation of IM-AGB stars supports a scenario where a fraction of the presently observed stars was formed from polluted or heavily polluted intracluster gas.

- In this regard, the distribution function of stars in [O/Na] for NGC 2808 is similar to the one seen in M 13, a template cluster as far as the the Na-O anticorrelation is concerned. This is interesting, since the HB morphology of these two clusters is very different.
- The average metallicity we found for NGC 2808 is $[Fe/H] = -1.10$ (rms = 0.065 dex, from 123 stars). We also found some evidence of a small intrinsic spread in metallicity, but more definitive conclusions are hampered by the presence of a small differential reddening.

Acknowledgements. This publication makes use of data products from the Two Micron All Sky Survey, which is a joint project of the University of Massachusetts and the Infrared Processing and Analysis Center/California Institute of Technology, funded by the National Aeronautics and Space Administration and the National Science Foundation. This work was partially funded by Cofin 2003029437 (P.I. Raffaele Gratton) "Continuità e discontinuità nella formazione della nostra Galassia" by the Ministero Università e Ricerca Scientifica, Italy.

References

- Alonso, A., Arribas, S., & Martinez-Roger, C. 1999, A&AS, 140, 261
- Alonso, A., Arribas, S., & Martinez-Roger, C. 2001, A&A, 376, 1039
- Bedin, L. R., Piotto, G., Zoccali, M., et al. 2000, A&A, 363, 159
- Böhm-Vitense, E. 1979, ApJ, 234, 521
- Bragaglia, A., Carretta, E., Gratton, R. G., et al. 2001, AJ, 121, 327
- Brown, J. A., Wallerstein, G., & Gonzalez, G. 1999, AJ, 118, 1245
- Cardelli, J. A., Clayton, G. C., & Mathis, J. S. 1989, ApJ, 345, 245
- Carretta, E. 1994, Ph.D. Thesis, University of Padova
- Carretta, E., & Gratton, R. G. 1997, A&AS, 121, 95
- Carretta, E., Cohen, J. G., Gratton, R. G., & Behr, B. B. 2001, AJ, 122, 1489
- Carretta, E., Bragaglia, A., Cacciari, C., & Rossetti, E. 2003, A&A, 410, 143
- Carretta, E., Bragaglia, A., & Cacciari 2004a, ApJ, 610, L25
- Carretta, E., Gratton, R. G., Bragaglia, A., Bonifacio, P., & Pasquini, L. 2004b, A&A, 416, 925
- Carretta, E., Gratton, R. G., Lucatello, S., Bragaglia, A., & Bonifacio, P. 2005, A&A, 433, 597
- Cohen, J. G. 2004, AJ, 127, 1545
- Cohen, J. G., & Melendez, J. 2005, AJ, 129, 303
- Cohen, J. G., Briley, M. M., & Stetson, P. B. 2002, AJ, 123, 2525
- Cottrell, P. L., & Da Costa, G. S. 1981, ApJ, 245, L79
- Cutri, R. M., et al. 2003, VizieR On-line Data Catalog: II/246, Originally published in: University of Massachusetts and Infrared Processing and Analysis Center (IPAC/California Institute of Technology)
- D'Antona, F., & Caloi, V. 2004, ApJ, 611, 871
- D'Antona, F., Caloi, V., Montalbán, J., Ventura, P., & Gratton, R. 2002, A&A, 395, 69
- D'Antona, F., Bellazzini, M., Caloi, V., et al. 2005, ApJ, 631, 868
- Denisenkov, P. A., & Denisenkova, S. N. 1989, A.Tsir., 1538, 11
- Gonzalez, G., & Wallerstein, G. 1998, AJ, 116, 765
- Gratton, R. G. 1988, Rome Obs. Preprint Ser., 29
- Gratton, R. G., Carretta, E., Eriksson, K., & Gustafsson, B. 1999, A&A, 350, 955
- Gratton, R. G., Bonifacio, P., Bragaglia, A., et al. 2001, A&A, 369, 87
- Gratton, R. G., Carretta, E., Claudi, R., Lucatello, S., & Barbieri, M. 2003, A&A, 404, 187
- Gratton, R. G., Sneden, C., & Carretta, E. 2004, ARA&A, 42, 385
- Harris, W. E. 1996, AJ, 112, 1487
- Ivans, I. I., Sneden, C., Kraft, R. P., et al. 1999, AJ, 118, 1273
- Ivans, I. I., Kraft, R. P., Sneden, C., et al. 2001, AJ, 122, 1438
- Kraft, R. P., Sneden, C., Langer, G. E., Shetrone, M. D., & Bolte, M. 1995, AJ, 109, 2586
- Kraft, R. P., Sneden, C., Smith, G. H., Shetrone, M. D., & Fulbright, J. 1998, AJ, 115, 1500
- Kurucz, R. L. 1995, CD-ROM 13, Smithsonian Astrophysical Observatory, Cambridge
- Langer, G. E., Hoffman, R., & Sneden, C. 1993, PASP, 105, 301
- Magain, P. 1984, A&A, 134, 189
- Moore, C. E., Minnaert, M. G. J., & Houtgast, J. 1966, The Solar Spectrum 2935 Å to 8770 Å (Washington: GPO)
- Norris, J. E., & Da Costa, G. S. 1995, ApJ, 441, L81
- Pasquini, L., Avila, G., Blecha, A., et al. 2002, The Messenger, 110, 1
- Ramirez, S., & Cohen, J. G. 2002, AJ, 123, 3277
- Shetrone, M. D., & Keane, M. J. 2000, AJ, 119, 840
- Smith, G. H., Sneden, C., & Kraft, R. P. 2002, AJ, 123, 1502
- Sneden, C., Kraft, R. P., Shetrone, M. D., et al. 1997, AJ, 114, 1964
- Sneden, C., Kraft, R. P., Guhathakurta, P., Peterson, R. C., & Fulbright, J. P. 2004, AJ, 127, 2162
- Tautvaisiene, G., Wallerstein, G., Geisler, D., Gonzalez, G., & Charbonnel, C. 2004, AJ, 127, 373
- Ventura, P., D'Antona, F., Mazzitelli, I., & Gratton, R. 2001, ApJ, 550, L65
- Walker, A. R. 1999, AJ, 118, 432
- Yong, D., Grundahl, F., Lambert, D. L., Nissen, P. E., & Shetrone, M. D. 2003, A&A, 402, 985

Online Material

Table 2. Information on the targets. B , V and coordinates at J2000 are taken from Bedin et al. (2000); J , K are from the 2MASS catalogue; RV 's for both gratings are heliocentric; stars with “*” in notes have $V - K$ colours that deviate from the ones expected for RGB stars, and have to be taken with caution.

Star	RA (h m s)	Dec (d p s)	V	B	J	K	$RV(HR11)$	$RV(HR13)$	HR	Notes
7183	9 12 2.8710	-64 49 34.069	14.854	16.168			106.58	106.55	11,13	
7315	9 11 58.581	-64 49 29.88	14.683	15.930	12.255	11.425	98.30	98.97	11,13	
7536	9 12 31.7065	-64 49 22.268	14.372	15.812	11.802	10.829		96.77	13	
7558	9 12 20.1287	-64 49 21.891	15.389	16.576	13.160	12.407	117.01	118.12	11,13	
7788	9 11 57.1979	-64 49 14.551	14.870	16.168	12.472	11.623	98.91		11	
8198	9 11 48.9714	-64 48 59.526	15.340	16.572	13.042	12.277	100.09		11	
8204	9 11 58.577	-64 48 59.27	15.119	16.397	12.793	11.879	109.67	109.95	11,13	
8603	9 12 14.0510	-64 48 42.915	14.432	15.847	11.902	10.957	109.93		11	
8679	9 11 44.5585	-64 48 39.890	14.961	16.164	12.753	12.022		43.27	13	Field
8739	9 11 51.2018	-64 48 37.535	14.288	15.761	11.620	10.693	110.50		11	
8826	9 12 9.8073	-64 48 33.243	15.033	16.275	12.746	11.911	96.33	96.56	11,13	
9230	9 12 13.3528	-64 48 11.617	14.028	15.591	11.252	10.303	88.81		11	
9724	9 12 0.9163	-64 47 43.204	14.508	15.869	11.994	11.090	90.17	89.75	11,13	
9785	9 11 55.6256	-64 47 39.790	15.346	16.493	13.197	12.471		25.35	13	Field
10012	9 11 58.5661	-64 47 23.138	14.225	15.682	11.613	10.679	109.26	109.39	11,13	
10105	9 12 21.1477	-64 47 13.906	14.669	15.976	12.279	11.417		117.95	13	
10265	9 11 56.6812	-64 47 0.535	14.309	15.728	11.772	10.823	112.39	112.32	11,13	
10341	9 12 25.4161	-64 46 52.409	14.659	16.009	12.205	11.335	102.39	103.15	11,13	
10571	9 12 41.1223	-64 46 25.848	14.376	15.806	11.771	10.844	109.43		11	
13575	9 11 31.6300	-64 49 2.281	15.386	16.615	13.090	12.270	95.10	95.14	11,13	
30523	9 11 22.4875	-64 55 23.351	15.489	16.658	13.320	12.550	96.46	96.79	11,13	
30720	9 11 28.0841	-64 55 1.802	15.387	16.557	13.229	12.491	96.62	96.80	11,13	
30763	9 11 31.6195	-64 54 57.989	14.606	15.927	12.287	11.465	97.33		11	
30873	9 11 9.0004	-64 54 49.625	14.821	15.995	12.710	11.936		45.02	13	*,Field
30900	9 11 36.3238	-64 54 47.078	15.084	16.319	12.890	12.075	116.56	116.03	11,13	
31361	9 11 33.3259	-64 54 9.237	15.204	16.405	13.051	12.229	94.63	93.39	11,13	
31823	9 11 30.7645	-64 53 37.745	13.946	15.437	11.430	10.540	112.42	110.29	11,13	
31851	9 11 14.3696	-64 53 36.046	15.221	16.420	13.064	12.280	100.11	100.01	11,13	
32398	9 11 39.4612	-64 53 1.270	14.687	16.004	12.321	11.483	96.95	97.15	11,13	
32469	9 11 16.3279	-64 52 55.955	14.040	15.485	11.531	10.689	102.11	102.08	11,13	
32909	9 11 39.6760	-64 52 31.924	15.022	16.272	12.710	11.910		96.68	13	
32924	9 11 22.2965	-64 52 31.081	14.853	16.138	12.515	11.701	98.79	98.36	11,13	
33452	9 11 40.7982	-64 52 1.561	15.170	16.405	12.970	12.167	93.92	94.14	11,13	
33918	9 11 1.6928	-64 51 36.087	14.331	15.776	11.756	10.887		117.17	13	
34008	9 11 27.5242	-64 51 31.290	15.119	16.346	12.894	12.115	103.59		11	
34634	9 11 25.2326	-64 50 53.601	15.361	16.594	13.143	12.310	107.58	106.88	11,13	
35265	9 11 22.7197	-64 50 12.117	15.321	16.584	12.965	12.180		100.13	13	
37496	9 12 13.8815	-64 57 9.411	14.871	16.126	12.586	11.730	112.51	112.72	11,13	
37505	9 12 26.4217	-64 57 8.391	14.783	16.058	12.471	11.591	100.53	100.26	11,13	
37781	9 12 13.0342	-64 56 41.142	15.037	16.148	13.001	12.307	76.17		11	*
37831	9 11 50.8459	-64 56 37.648	15.360	16.534	13.178	12.423	102.00	101.31	11,13	
37998	9 12 12.5554	-64 56 24.603	14.233	15.638	11.706	10.796	93.69	93.44	11,13	
38228	9 12 30.9696	-64 56 8.521	14.981	16.211	12.700	11.887		102.77	13	
38244	9 12 8.9333	-64 56 7.955	15.193	16.378	12.996	12.177		109.83	13	
38559	9 12 56.1453	-64 55 48.356	14.133	15.541	11.674	10.754	-14.07	-15.26	11,13	Field
38660	9 12 39.8673	-64 55 43.083	14.290	15.672	11.785	10.875	98.85		11	
38967	9 12 8.8682	-64 55 27.764	15.252	16.415	13.060	12.297	97.28		13	
39060	9 12 14.5222	-64 55 24.085	14.417	15.793	11.939	11.036	115.79	115.58	11,13	
39577	9 12 10.9820	-64 55 3.959	14.509	15.820	12.085	11.189	250.70		11	Field
40983	9 11 48.6726	-64 54 20.737	14.360	15.723	11.906	10.988	116.62	115.90	11,13	
41008	9 12 17.6744	-64 54 19.865	15.189	16.339	12.973	12.200	93.84	94.32	11,13	
41050	9 12 3.3926	-64 54 18.758	14.502	15.840	12.011	11.171	107.09	106.97	11,13	
41207	9 11 54.9517	-64 54 14.760	13.997	15.478	11.358	10.423	110.75	110.61	11,13	
41688	9 12 35.2695	-64 54 3.795	15.089	16.293	12.797	11.982	122.12	121.14	11,13	
41828	9 12 8.5555	-64 54 0.670	14.521	15.862	12.129	11.210	100.28	100.45	11,13	

Table 2. continued.

Star	RA (h m s)	Dec (d p s)	<i>V</i>	<i>B</i>	<i>J</i>	<i>K</i>	<i>RV</i> (HR11)	<i>RV</i> (HR13)	HR	Notes
41969	9 11 50.8999	-64 53 57.615	14.446	15.787	11.972	11.092	89.23	88.87	11,13	
42122	9 12 17.6820	-64 53 54.285	14.708	16.011	12.276	11.375		111.94	13	
42996	9 12 25.0560	-64 53 37.226	15.426	16.552	13.294	12.523		91.86	13	
43097	9 11 56.602	-64 53 35.56	15.370	16.460	13.251	12.570	99.93	100.38	11,13	
43194	9 12 11.0494	-64 53 33.711	14.595	15.876	12.252	11.369	114.36		11	
43247	9 12 10.1184	-64 53 32.654	14.786	16.022	12.486	11.543		109.75	13	
43333	9 12 55.0733	-64 53 30.392	15.473	16.570	13.408	12.698	-15.45	-16.83	11,13	Field
43794	9 12 26.3414	-64 53 22.607	14.554	15.861	12.157	11.271	101.91	101.45	11,13	
43972	9 12 4.113	-64 53 19.75	15.270	16.379	13.121	12.354	99.25		11	
44213	9 11 46.6745	-64 53 15.425	15.266	16.413	13.056	12.251	95.31		11	
44526	9 12 10.9800	-64 53 9.950	15.459	16.540				102.60	13	
44665	9 12 15.2786	-64 53 7.367	14.245	15.649	11.718	10.799	93.26	92.82	11,13	
44716	9 12 17.8493	-64 53 6.449	14.899	16.123	12.605	11.748	102.12		11	
44984	9 12 45.8780	-64 53 1.411	14.535	15.855	12.088	11.219		89.89	13	
44996	9 11 56.3602	-64 53 1.850	14.391	15.773	11.898	10.993	85.39	83.47	11,13	
45443	9 12 21.3723	-64 52 54.137	14.574	15.885	12.128	11.283	100.97	101.35	11,13	
45496	9 11 58.9127	-64 52 53.509	14.485	15.799	12.058	11.126		103.27	13	
45530	9 12 3.4358	-64 52 52.758	14.737	15.984	12.389	11.545	108.58		11	
45701	9 11 51.1173	-64 52 49.961	15.025	16.231	12.701	11.884		90.23	13	
46036	9 11 45.8526	-64 52 44.443	14.532	15.810	12.144	11.268	111.94	111.26	11,13	
46520	9 12 13.2216	-64 52 36.335	15.448	16.583	13.323	12.606		88.06	13	
46587	9 11 54.1303	-64 52 35.209	14.488	15.815	11.993	11.039		103.36	13	
46663	9 12 17.0998	-64 52 33.946	14.551	15.860	12.146	11.323	95.98	95.72	11,13	
46800	9 11 51.373	-64 52 31.73	13.931	15.423	11.335	10.394	103.95		11	
46868	9 12 9.7828	-64 52 30.452	14.752	16.003			110.23	109.88	11,13	
46908	9 12 7.0175	-64 52 29.772	14.264	15.636	11.808	10.905	93.52	92.96	11,13	
46924	9 12 4.6008	-64 52 29.587	14.826	16.096				99.44	13	
47071	9 11 56.5195	-64 52 27.093	14.605	15.845	12.292	11.338	112.23		11	
47421	9 11 56.4377	-64 52 21.270	14.175	15.571	11.674	10.696		74.86	13	
47502	9 11 51.6422	-64 52 19.859	14.113	15.521	11.584	10.658	88.20	87.70	11,13	
47638	9 12 3.6988	-64 52 17.777	14.337	15.641			102.86		11	
47667	9 12 9.4941	-64 52 17.455	14.444	15.817	11.960	11.033	109.80		11	
47700	9 12 1.0750	-64 52 16.983	14.810	16.039	12.532	10.470	102.89		11	*
47805	9 11 59.0036	-64 52 15.455	14.152	15.548	11.712	10.748	104.73	104.80	11,13	
48001	9 12 25.6290	-64 52 12.098	15.234	16.394	13.018	12.236		109.11	13	
48011	9 11 48.0108	-64 52 12.236	14.397	15.718	11.965	11.040	101.07	101.08	11,13	
48424	9 12 6.6195	-64 52 5.871	14.452	15.772	11.995	9.519	111.87	111.54	11,13	*
49122	9 11 55.3947	-64 51 54.883	15.027	16.253	12.714	11.859		101.96	13	
49493	9 11 52.9145	-64 51 49.274	15.143	16.321	12.935	12.119	99.36	98.53	11,13	
49743	9 12 36.7974	-64 51 45.097	15.168	16.353	12.925	12.159	113.11		11	
49753	9 12 6.8961	-64 51 45.474	14.350	15.669	11.804	10.886	118.42	118.40	11,13	
50119	9 11 42.9184	-64 51 39.752	13.886	15.425	11.210	10.218	100.96		11	
50561	9 12 23.1839	-64 51 32.695	14.834	16.120	12.428	11.548	95.00		11	
50685	9 12 13.8767	-64 51 30.699	14.551	15.872	11.579	10.80	108.16	107.76	11,13	*
50866	9 11 54.2702	-64 51 27.928	14.634	15.941	12.219	11.353	94.40		11	
50910	9 11 42.6346	-64 51 27.221	14.984	16.234	12.697	11.877		96.94	13	
51256	9 11 55.1950	-64 51 21.739	14.567	15.876	12.186	11.302		127.42	13	
51416	9 12 29.2944	-64 51 18.935	14.945	16.188	12.619	11.803	91.02		11	
51519	9 11 56.818	-64 51 17.50	14.146	15.540	11.545	10.677	112.33	111.60	11,13	
51646	9 11 50.3432	-64 51 15.395	15.460	16.550	13.425	12.668	99.41		11	
51918	9 12 8.5198	-64 51 11.051	14.187	15.626				97.26	13	
51930	9 11 49.9340	-64 51 10.872	14.068	15.531	11.422	10.478		91.76	13	
51963	9 12 27.6355	-64 51 10.138	14.199	15.652	11.577	10.652	103.64		11	
52006	9 12 18.1017	-64 51 9.524	14.322	15.653	11.945	10.995	110.99	111.51	11,13	
52048	9 12 5.7704	-64 51 8.996	14.259	15.645	10.387	10.797	77.03	77.09	11,13	
52083	9 12 8.5727	-64 51 8.436	15.408	16.571			110.92		11	
52647	9 12 12.2817	-64 50 59.590	14.654	15.925	12.293	11.432	124.62	124.31	11,13	
52891	9 12 3.1668	-64 50 55.709	14.426	15.721	11.980	11.072	83.23	83.16	11,13	

Table 2. continued.

Star	RA (h m s)	Dec (d p s)	<i>V</i>	<i>B</i>	<i>J</i>	<i>K</i>	<i>RV</i> (HR11)	<i>RV</i> (HR13)	HR	Notes
53209	9 11 59.2764	-64 50 50.638	14.427	15.778	12.070	11.114		102.49	13	
53284	9 12 1.4868	-64 50 49.350	13.847	15.501	10.902	9.953	107.04	105.07	11,13	
53579	9 11 48.7436	-64 50 44.801	14.461	15.830	11.877	10.992	96.78		11	
53629	9 12 6.588	-64 50 43.90	15.340	16.443			103.85	103.10	11,13	
54264	9 12 21.5127	-64 50 33.737	15.336	16.475	13.193	12.329	120.88	120.33	11,13	
54266	9 11 50.134	-64 50 33.92	14.790	16.028	12.465	11.593	111.25		11	
54284	9 11 54.7689	-64 50 33.662	14.407	15.789	11.877	10.985	115.95	115.59	11,13	
54644	9 12 2.0927	-64 50 28.127	15.347	16.513	13.141	12.412		112.91	13	
54756	9 11 46.3335	-64 50 26.044	14.784	16.086	12.416	11.528	95.95	95.49	11,13	
54789	9 12 0.4239	-64 50 25.567	14.247	15.626	11.756	10.863	95.44		11	
55354	9 12 10.3337	-64 50 16.108	14.749	16.024	12.406	11.531	112.63	112.42	11,13	
55609	9 12 29.9315	-64 50 11.384	14.751	16.078	12.301	11.467	116.19	116.27	11,13	
55822	9 12 12.1771	-64 50 7.930	15.421	16.494	13.276	12.595		99.96	13	
56032	9 11 45.5811	-64 50 4.209	13.976	15.579	11.112	10.095	90.11		11	
56103	9 12 1.8250	-64 50 3.003	15.347	16.502	13.211	12.356	104.27		11	
56710	9 12 30.1594	-64 49 52.049	15.430	16.582	13.232	12.396	114.28	113.69	11,13	
56924	9 12 15.1423	-64 49 48.859	14.207	15.629	11.587	10.676	101.71	102.00	11,13	

Table 3. Adopted atmospheric parameters and derived Iron abundances; nr indicates the number of lines used in the analysis.

Star	T_{eff} (K)	$\log g$ (dex)	[A/H] (dex)	v_t (km s ⁻¹)	nr	[Fe/H]I (dex)	rms	nr	[Fe/H]II (dex)	rms
07183	4423	1.51	-1.08	1.66	41	-1.08	0.13	3	-1.06	0.17
07315	4452	1.45	-1.24	1.54	33	-1.24	0.10	3	-1.16	0.17
07536	4247	1.18	-1.09	1.45	23	-1.08	0.13	3	-1.01	0.11
07558	4692	1.87	-1.22	1.30	33	-1.21	0.12	3	-1.17	0.18
07788	4461	1.53	-1.17	1.40	18	-1.17	0.14			
08198	4617	1.81	-1.21	1.21	13	-1.21	0.14			
08204	4467	1.63	-1.05	1.35	38	-1.05	0.15	3	-1.14	0.14
08603	4292	1.24	-1.05	1.65	19	-1.05	0.12			
08679	4734	1.72	-0.25	1.38	21		0.20	3	-0.79	0.07
08739	4213	1.13	-1.07	1.82	19	-1.07	0.12			
08826	4565	1.66	-0.99	1.22	39	-0.98	0.15	3	-0.97	0.08
09230	4134	0.96	-1.21	1.57	17	-1.22	0.08			
09724	4332	1.30	-1.15	1.30	41	-1.15	0.15	3	-1.22	0.10
09785	4799	1.91	-0.67	1.31	23		0.14	3	-1.07	0.18
10012	4245	1.12	-1.05	1.73	41	-1.06	0.15	4	-1.02	0.25
10105	4457	1.45	-1.20	1.34	21	-1.21	0.12	3	-1.27	0.09
10265	4285	1.19	-1.03	1.51	37	-1.04	0.15	3	-1.08	0.13
10341	4401	1.41	-1.09	1.35	37	-1.09	0.11	3	-1.14	0.18
10571	4254	1.19	-1.08	1.80	19	-1.08	0.13			
13575	4570	1.80	-1.23	1.20	36	-1.22	0.13	4	-1.16	0.23
30523	4734	1.94	-1.14	1.60	29	-1.14	0.11	3	-1.23	0.10
30720	4777	1.92	-1.19	1.30	31	-1.18	0.11	2	-1.15	0.07
30763	4549	1.48	-1.06	1.66	18	-1.06	0.08			
30873	4645	1.61	-0.41	1.41	22		0.17	4	-0.80	0.28
30900	4667	1.74	-1.13	1.36	35	-1.14	0.14	3	-1.20	0.18
31361	4700	1.80	-1.06	1.24	37	-1.07	0.13	2	-1.17	0.16
31823	4341	1.08	-1.17	1.69	33	-1.17	0.11	3	-1.19	0.15
31851	4732	1.83	-1.09	1.30	37	-1.08	0.14	2	-1.16	0.10
32398	4496	1.48	-1.12	1.44	36	-1.12	0.09	3	-1.11	0.14
32469	4381	1.14	-1.21	2.27	39	-1.21	0.10	3	-1.21	0.08
32909	4574	1.66	-1.04	1.37	20	-1.03	0.13	3	-1.06	0.10
32924	4539	1.57	-1.18	1.91	37	-1.18	0.09	3	-1.22	0.07
33452	4673	1.78	-1.10	1.24	40	-1.10	0.16	3	-1.29	0.08
33918	4313	1.22	-1.05	1.61	22	-1.05	0.16	3	-1.06	0.16
34008	4672	1.75	-1.00	1.75	14	-1.00	0.10			
34634	4628	1.83	-1.18	1.10	33	-1.18	0.13	3	-1.28	0.19
35265	4548	1.76	-1.14	1.21	23	-1.15	0.16	3	-1.16	0.18
37496	4549	1.58	-1.05	1.80	37	-1.06	0.13	3	-1.17	0.11
37505	4506	1.52	-1.12	1.92	38	-1.12	0.11	3	-1.09	0.06
37781	4752	1.78	-0.32	1.37	15		0.07			
37831	4736	1.88	-1.17	1.30	40	-1.17	0.13	3	-1.40	0.04
37998	4319	1.18	-1.07	1.78	43	-1.07	0.14	3	-1.19	0.13
38228	4590	1.65	-1.03	1.32	23	-1.03	0.13	3	-1.05	0.22
38244	4661	1.78	-1.20	1.24	22	-1.21	0.14	3	-1.27	0.15
38559	4360	1.17	-0.25	1.55	33		0.17	2	-0.84	0.01
38660	4334	1.21	-1.00	1.92	20	-1.01	0.11			
38967	4719	1.83	-1.19	1.23	22	-1.19	0.17	3	-1.47	0.21
39060	4359	1.28	-1.01	1.39	39	-1.01	0.13	3	-1.11	0.11
39577	4404	1.35	-0.69	1.48	19		0.15			
40983	4365	1.26	-1.02	1.41	38	-1.02	0.13	3	-1.11	0.13
41008	4686	1.79	-1.06	1.14	38	-1.05	0.17	2	-1.11	0.14
41050	4396	1.34	-1.04	1.38	40	-1.04	0.13	3	-1.15	0.19
41207	4226	1.02	-1.19	1.57	36	-1.20	0.11	2	-1.18	0.06
41688	4578	1.69	-1.00	1.36	39	-1.01	0.14	3	-1.09	0.10
41828	4411	1.36	-1.08	1.47	42	-1.08	0.13	3	-1.25	0.17
41969	4379	1.31	-1.05	1.25	40	-1.05	0.14	3	-1.16	0.14
42122	4394	1.42	-1.12	1.54	18	-1.12	0.12	3	-1.11	0.22

Table 3. continued.

Star	T_{eff} (K)	$\log g$ (dex)	[A/H] (dex)	v_r (km s ⁻¹)	nr	[Fe/H]I (dex)	rms	nr	[Fe/H]II (dex)	rms
42996	4770	1.93	-1.12	1.49	18	-1.11	0.17	3	-1.26	0.05
43097	4878	1.96	-1.06	1.50	36	-1.05	0.16	3	-1.26	0.13
43194	4478	1.43	-1.01	1.46	20	-1.01	0.09			
43247	4465	1.50	-1.04	1.62	22	-1.03	0.14	3	-1.05	0.17
43333	4906	2.02	-0.25	1.28	39		0.15	3	-0.46	0.53
43794	4433	1.38	-1.09	1.49	41	-1.09	0.14	3	-1.03	0.21
43972	4757	1.86	-1.14	1.32	17	-1.13	0.14			
44213	4662	1.81	-1.13	1.32	16	-1.13	0.11			
44526	4805	1.97	-1.07	1.48	17	-1.06	0.16	3	-1.20	0.10
44665	4312	1.18	-1.06	1.73	40	-1.06	0.14	3	-1.09	0.20
44716	4540	1.59	-1.10	1.40	18	-1.10	0.14			
44984	4407	1.36	-1.22	1.47	23	-1.23	0.14	3	-1.17	0.29
44996	4346	1.26	-1.03	1.30	41	-1.03	0.15	3	-1.15	0.16
45443	4426	1.39	-1.08	1.36	38	-1.07	0.11	2	-1.15	0.13
45496	4375	1.32	-1.15	1.28	21	-1.16	0.12	3	-1.18	0.12
45530	4506	1.50	-1.14	1.43	17	-1.15	0.08			
45701	4549	1.64	-0.98	1.27	23	-0.99	0.14	3	-1.07	0.11
46036	4448	1.38	-1.04	1.47	41	-1.01	0.14	4	-0.99	0.23
46520	4833	1.97	-1.03	1.03	11	-1.03	0.10	2	-1.09	0.22
46587	4310	1.28	-1.20	1.28	22	-1.20	0.15	3	-1.11	0.09
46663	4476	1.41	-1.05	1.47	41	-1.06	0.14	3	-1.25	0.09
46800	4250	1.01	-1.20	1.29	15	-1.20	0.08			
46868	4521	1.53	-1.16	1.55	35	-1.16	0.09	3	-1.19	0.28
46908	4375	1.23	-1.08	1.62	40	-1.08	0.12	3	-1.20	0.03
46924	4491	1.54	-1.11	1.61	23	-1.11	0.17	3	-1.16	0.07
47071	4446	1.41	-1.13	1.46	19	-1.13	0.10			
47421	4290	1.14	-1.10	1.79	21	-1.11	0.13	3	-1.18	0.11
47502	4306	1.12	-1.12	1.95	38	-1.12	0.13	2	-1.14	0.08
47638	4439	1.31	-1.09	1.51	19	-1.09	0.14			
47667	4337	1.28	-0.99	1.69	18	-0.99	0.09			
47700	4556	1.57	-1.14	1.22	19	-1.14	0.09			
47805	4342	1.16	-1.13	1.85	39	-1.13	0.11	3	-1.19	0.12
48001	4677	1.80	-1.18	1.33	20	-1.18	0.11	4	-1.15	0.28
48011	4376	1.28	-1.01	1.40	37	-1.01	0.15	3	-1.03	0.12
48424	4415	1.34	-1.05	1.29	41	-1.06	0.15	3	-1.09	0.09
49122	4526	1.63	-1.04	1.37	21	-1.04	0.11	3	-1.10	0.02
49493	4653	1.75	-1.17	1.30	39	-1.16	0.17	4	-1.24	0.14
49743	4667	1.77	-1.07	1.74	16	-1.07	0.12			
49753	4300	1.21	-1.12	1.21	40	-1.11	0.15	3	-1.16	0.10
50119	4168	0.93	-1.11	1.80	18	-1.11	0.09			
50561	4430	1.49	-1.20	1.21	14	-1.20	0.06			
50685	4413	1.38	-1.05	1.47	42	-1.05	0.14	3	-1.04	0.15
50866	4434	1.42	-1.10	1.45	19	-1.10	0.09			
50910	4578	1.65	-1.15	1.38	20	-1.15	0.12	3	-1.17	0.08
51256	4447	1.40	-1.10	1.37	16	-1.10	0.10	2	-1.07	0.26
51416	4548	1.61	-1.01	1.39	17	-1.02	0.14			
51519	4296	1.13	-1.17	1.75	37	-1.16	0.13	3	-1.09	0.02
51646	4887	2.00	-1.16	1.48	17	-1.16	0.11			
51918	4243	1.12	-1.14	1.84	22	-1.14	0.14	3	-1.13	0.21
51930	4216	1.04	-1.13	1.86	23	-1.13	0.17	3	-1.16	0.11
51963	4244	1.11	-1.09	1.54	18	-1.10	0.14			
52006	4399	1.27	-1.01	1.51	34	-1.01	0.13	3	-1.05	0.14
52048	4296	1.17	-1.08	1.62	43	-1.08	0.13	3	-1.18	0.09
52083	4664	1.88	-1.11	1.09	13	-1.22	0.09			
52647	4481	1.45	-1.07	1.25	30	-1.07	0.08	3	-1.31	0.14
52891	4379	1.30	-1.08	1.19	40	-1.08	0.15	3	-1.28	0.16

Table 3. continued.

Star	T_{eff} (K)	$\log g$ (dex)	[A/H] (dex)	v_t (km s ⁻¹)	nr	[Fe/H]I (dex)	rms	nr	[Fe/H]II (dex)	rms
53209	4410	1.32	-1.11	1.39	23	-1.10	0.14	3	-1.21	0.13
53284	4040	0.81	-1.13	2.00	37	-1.13	0.13	3	-1.01	0.15
53579	4296	1.26	-1.02	1.59	19	-1.02	0.13			
53629	4767	1.90	-1.11	1.21	31	-1.11	0.16	1	-1.55	
54264	4669	1.84	-1.21	1.11	38	-1.20	0.15	3	-1.41	0.13
54266	4502	1.52	-1.22	1.22	15	-1.22	0.07			
54284	4329	1.26	-1.05	1.40	41	-1.05	0.16	3	-1.14	0.20
54644	4738	1.88	-1.16	1.11	21	-1.15	0.13	3	-1.40	0.09
54756	4454	1.49	-1.17	1.82	36	-1.17	0.09	3	-1.08	0.14
54789	4356	1.21	-1.00	1.53	17	-1.00	0.15			
55354	4484	1.49	-1.04	1.53	32	-1.04	0.10	3	-1.04	0.19
55609	4432	1.46	-1.07	1.73	37	-1.06	0.10	3	-1.13	0.15
55822	4850	1.97	-1.06	1.39	17	-1.05	0.11	3	-1.22	0.19
56032	4047	0.87	-1.10	1.58	19	-1.11	0.11			
56103	4684	1.85	-1.18	1.31	15	-1.17	0.12			
56710	4644	1.86	-1.18	1.39	32	-1.18	0.12	4	-1.21	0.18
56924	4254	1.12	-1.10	1.84	41	-1.10	0.13	3	-1.13	0.09

Table 5. Abundances of O and Na in NGC 2808. [Na/Fe] values are corrected for departures from LTE. HR is a flag for the grating used for the observations (2 = HR 11 and HR 13, 1 = HR 11 only, 3 = HR 13 only). Lim is a flag for detection or upper limit in the O measurements (0 = upper limit, 1 = detection).

Star	nr	[O/Fe]	rms	nr	[Na/Fe]	rms	HR	lim
07183	2	+0.109	0.285	4	+0.217	0.093	2	1
07315	2	+0.384	0.041	4	-0.132	0.069	2	1
07536	2	+0.386	0.049	2	+0.004	0.067	1	1
07558	2	+0.428	0.205	2	+0.041	0.063	2	1
07788				2	+0.503	0.102	3	1
08198				2	+0.126	0.029	3	1
08204	2	+0.324	0.004	4	-0.010	0.162	2	1
08603				2	+0.052	0.143	3	1
08679	2	-0.136	0.028	2	+0.303	0.036	1	1
08739				2	+0.101	0.053	3	1
08826	1	-0.605		3	+0.470	0.167	2	1
09230				2	+0.659	0.081	3	1
09724	2	-0.171	0.091	4	+0.426	0.181	2	1
09785				2	+0.471	0.027	1	1
10012	2	-0.235	0.164	4	+0.369	0.151	2	1
10105	2	+0.366	0.012	2	-0.118	0.019	1	1
10265	2	-0.193	0.047	4	+0.409	0.167	2	1
10341	1	-0.876		4	+0.531	0.089	2	0
10571				2	+0.352	0.141	3	1
13575	2	+0.284	0.024	3	-0.043	0.017	2	1
30523	2	+0.400	0.006	3	-0.026	0.113	2	1
30720	2	+0.334	0.078	3	-0.028	0.067	2	1
30763				2	+0.427	0.077	3	1
30873	2	-0.145	0.098	2	+0.485	0.026	1	1
30900	2	+0.346	0.035	3	+0.109	0.148	2	1
31361	2	-0.544	0.155	4	+0.580	0.138	2	0
31823	2	-0.362	0.095	4	+0.426	0.154	2	1
31851	1	-0.610		4	+0.573	0.117	2	1
32398	2	+0.184	0.084	4	-0.034	0.116	2	1
32469	2	+0.140	0.093	4	+0.363	0.117	2	1
32909	2	-0.192	0.146	2	+0.312	0.000	1	1
32924	1	+0.286		4	+0.469	0.083	2	1
33452	2	+0.389	0.070	4	-0.037	0.161	2	1
33918	2	+0.314	0.066	2	+0.071	0.037	1	1
34008				2	+0.631	0.100	3	1
34634	2	+0.333	0.031	3	-0.068	0.108	2	1
35265	2	+0.381	0.004	1	-0.063		1	1
37496	2	+0.350	0.199	4	+0.023	0.052	2	1
37505	2	+0.218	0.026	4	+0.064	0.088	2	1
37781				2	+0.604	0.083	3	1
37831	2	+0.448	0.077	4	+0.085	0.129	2	1
37998	2	+0.386	0.071	4	+0.168	0.167	2	1
38228	2	+0.452	0.110	2	+0.016	0.091	1	1
38244	2	+0.461	0.072	2	+0.069	0.069	1	1
38559	2	-0.279	0.071	4	+0.691	0.173	2	1
38660				2	+0.099	0.123	3	1
38967	2	+0.230	0.177	2	+0.090	0.073	1	1
39060	2	+0.274	0.000	4	+0.148	0.159	2	1
39577				2	+0.466	0.042	3	1
40983	2	-0.541	0.269	4	+0.380	0.179	2	1
41008	1	-0.414		3	+0.696	0.175	2	1
41050	2	+0.264	0.035	4	+0.034	0.128	2	1
41207	2	+0.292	0.047	4	+0.083	0.095	2	1
41688	1	-0.233		4	+0.425	0.152	2	1

Table 5. continued.

Star	nr	[O/Fe]	rms	nr	[Na/Fe]	rms	HR	lim
41828	2	+0.115	0.018	4	+0.166	0.080	2	1
41969	2	+0.293	0.049	4	-0.029	0.179	2	1
42122	2	+0.263	0.037	2	+0.172	0.042	1	1
42996	2	-0.151	0.132	2	+0.523	0.016	1	1
43097	1	-0.399		4	+0.440	0.145	2	1
43194				2	+0.327	0.172	3	1
43247	2	-0.568	0.292	2	+0.378	0.028	1	1
43333				4	+0.432	0.063	2	1
43794	2	+0.430	0.047	4	-0.111	0.128	2	1
43972				2	+0.259	0.047	3	1
44213				2	+0.239	0.036	3	1
44526	2	-0.460	0.152	2	1.014	0.143	1	0
44665	2	+0.174	0.013	3	+0.285	0.108	2	1
44716				2	+0.704	0.096	3	1
44984	2	+0.395	0.126	2	+0.014	0.008	1	1
44996	2	+0.202	0.008	3	+0.131	0.141	2	1
45443	2	+0.303	0.033	4	-0.046	0.131	2	1
45496	2	-0.390	0.161	2	+0.300	0.006	1	1
45530				2	+0.529	0.121	3	1
45701	2	+0.222	0.013	2	+0.058	0.029	1	1
46036	2	+0.375	0.013	4	-0.132	0.118	2	1
46520	2	-0.532	0.243	2	+0.800	0.086	1	0
46587	2	-0.770	0.154	2	+0.690	0.015	1	0
46663	2	-0.782	0.314	4	+0.476	0.114	2	0
46800				2	+0.454	0.157	3	1
46868	2	+0.218	0.035	4	+0.182	0.157	2	1
46908	2	+0.253	0.037	3	+0.270	0.120	2	1
46924	2	+0.040	0.009	2	+0.327	0.001	1	1
47071				2	+0.320	0.032	3	1
47421	2	+0.009	0.177	2	+0.392	0.019	1	1
47502	2	-0.821	0.115	4	+0.628	0.132	2	1
47638				2	+0.781	0.047	3	1
47667				2	+0.322	0.040	3	1
47700				2	+0.454	0.060	3	1
47805	2	+0.184	0.108	4	+0.387	0.092	2	1
48001	2	+0.145	0.073	2	+0.316	0.009	1	1
48011	2	-0.829	0.084	4	+0.650	0.182	2	0
48424	2	+0.265	0.053	3	+0.131	0.099	2	1
49122	1	+0.311		2	+0.189	0.041	1	1
49493	2	+0.438	0.038	3	+0.115	0.162	2	1
49743				2	+0.517	0.128	3	1
49753	2	+0.156	0.004	3	+0.230	0.083	2	1
50119				2	+0.665	0.156	3	1
50561				2	+0.402	0.137	3	1
50685	2	+0.402	0.031	4	-0.134	0.143	2	1
50866				2	+0.450	0.042	3	1
50910	2	-0.126	0.177	2	+0.397	0.031	1	1
51256	2	+0.042	0.021	2	+0.372	0.124	1	1
51416				2	+0.711	0.131	3	1
51519	2	+0.517	0.027	3	+0.031	0.127	2	1
51646				2	+0.788	0.111	3	1
51918	1	-0.692		2	+0.590	0.031	1	1
51930	2	-0.006	0.024	2	+0.407	0.031	1	1
51963				2	+0.339	0.086	3	1
52006	2	-0.943	0.245	3	+0.635	0.177	2	0
52048	2	+0.312	0.203	4	+0.114	0.098	2	1

Table 5. continued.

Star	nr	[O/Fe]	rms	nr	[Na/Fe]	rms	HR	lim
52083				2	+0.214	0.002	3	1
52647	2	+0.219	0.020	4	-0.009	0.130	2	1
52891	2	+0.016	0.051	4	+0.177	0.159	2	1
53209	1	-0.374		2	+0.391	0.028	1	1
53284	2	+0.468	0.035	4	-0.087	0.178	2	1
53579				2	-0.006	0.065	3	1
53629	2	+0.388	0.037	2	-0.019	0.074	2	1
54264	2	+0.149	0.064	4	+0.167	0.074	2	1
54266				2	+0.082	0.124	3	1
54284	2	+0.171	0.045	4	+0.242	0.181	2	1
54644	2	+0.223	0.015	1	-0.143		1	1
54756	2	+0.005	0.000	4	+0.297	0.108	2	1
54789				2	1.116	0.076	3	1
55354	2	-0.346	0.120	4	+0.434	0.096	2	1
55609	2	+0.237	0.011	4	+0.046	0.141	2	1
55822	2	-0.517	0.243	2	+0.773	0.055	1	0
56032				2	+0.063	0.074	3	1
56103				2	+0.348	0.013	3	1
56710	2	+0.375	0.076	4	+0.062	0.159	2	1
56924	2	+0.246	0.168	4	+0.263	0.045	2	1